Atmos. Chem. Phys. Discuss., https://doi.org/10.5194/acp-2019-299
Manuscript under review for journal Atmos. Chem. Phys.
Discussion started: 24 April 2019

Atmospheric Chemistry and Physics Discussions

Chemical composition of ultrafine aerosol particles in central Amazonia during the wet season

Hayley S. Glicker[1], Michael J. Lawler[1], John Ortega[1], Suzane S. de Sá[2], Scot T. Martin[2,3], Paulo Artaxo[4], Oscar Vega Bustillos[5], Rodrigo de Souza[6], Julio Tota[7], Annmarie Carlton[1], and James N. Smith[1*]

[1] Department of Chemistry, University of California, Irvine, CA 92697 USA
[2] School of Engineering and Applied Sciences, Harvard University, Cambridge, Massachusetts 02138 USA
[3] Department of Earth and Planetary Sciences, Harvard University, Cambridge, Massachusetts 02138 USA
[4] Institute of Physics, University of São Paulo, Rua do Matão 1371, 05508-090, São Paulo, Brazil
[5] Instituto de Pesquisas Energéticas e Nucleares, São Paulo, Brazil
[6] Universidade do Estado do Amazonas, Manaus, AM, Brazil
[7] Institute of Engineering and Geoscience, Federal University of West Pará, Santarém, PA, Brazil

Correspondence to: James N. Smith (jimsmith@uci.edu)

Abstract Central Amazonia serves as an ideal location to study atmospheric particle formation since it often can be characterized as representing natural, pre-industrial conditions but can also experience periods of anthropogenic influence due to the presence of emissions from large metropolitan areas like Manaus, Brazil. Ultrafine (sub-100 nm diameter) particles are often observed in this region, although new particle formation events seldom occur near the ground despite being readily observed in other forested regions with similar emissions. This study focuses on identifying the chemical composition of ultrafine particles as a means of determining the chemical species and mechanisms that may be responsible for new particle formation and growth in the region. These measurements were performed during the wet season as part of the GoAmazon2014/5 field campaign at a site located 70 km southwest of Manaus. A Thermal Desorption Chemical Ionization Mass Spectrometer (TDCIMS) measured the concentrations of the most abundant compounds detected in ultrafine particles. Two time periods representing distinct influences on aerosol composition, which we label as "anthropogenic" and "background" periods, were studied as part of a larger ten-day period of analysis. The anthropogenic period saw higher particle number concentrations and modeled back-trajectories indicate transport of emissions from the Manaus metropolitan area. The background period saw much lower number concentrations and back-trajectories showed that air masses arrived at the site predominantly from the forested regions to the north and northeast. TDCIMS-measured constituents also show distinct differences between the two observational periods. Although bisulfate was detected in particles during the ten-day period, the anthropogenic period had increased levels of particulate bisulfate overall. Additionally, with larger fractions of bisulfate observed, increased fractions of ammonium and trimethyl ammonium were observed. The background period had distinct diurnal patterns of particulate organic nitrogen species and acetate, while oxalate remained relatively constant during the ten-day period. 3-Methylfuran, a thermal decomposition product of particulate phase isoprene epoxydiol (IEPOX), was the dominant species measured in the positive ion mode. Principal Component Analysis (PCA) was performed on the TDCIMS-measured ion abundance and Aerosol Mass Spectrometer (AMS) mass concentration data. Two different hierarchical clusters representing unique influences arise: one relating ultrafine particulate acetate, hydrogen oxalate, organic nitrogen species, trimethyl ammonium and 3-methylfuran with each

other and ultrafine particulate bisulfate, chloride, ammonium and potassium. A third cluster separated AMS-measured species from the two TDCIMS-derived clusters, indicating different sources or processes in ultrafine aerosol particle formation compared to submicron-sized particles.

1. Introduction

Atmospheric aerosols are ubiquitous in the troposphere, of which organics contribute a large fraction to the chemical composition (Jimenez et al., 2009). Models continue to have difficulty estimating the organic contribution to aerosols in regions with both biogenic and anthropogenic influence (Shrivastava et al., 2017). Anthropogenic emissions have increased with global population and the resulting influences of such emissions on secondary organic aerosol (SOA) formation continue to be assessed (Hofmann, 2015). The reactive chemistry of organics in the presence of different regulating species from urban sources, like sulfur dioxide (SO_2) and oxides of nitrogen, remains uncertain (Shrivastava et al., 2017), although recent efforts have successfully incorporated this chemistry into air quality models simulated for the southeastern United States (Carlton et al., 2018). Models are unable to predict the impacts of particle physical and chemical properties on cloud formation and precipitation (IPCC, 2013). Reducing this uncertainty would be aided by an understanding of the mechanisms by which particles form and grow in the atmosphere, which mostly determine the potential of these particles to serve as cloud condensation nuclei (CCN).

The Amazon basin is an ideal location to study how biogenic emissions, anthropogenic trace gases and oxidants, and biomass burning impact the number and composition of atmospheric aerosol particles. The Amazon basin is one of the few remaining tropical regions on Earth in which near-natural conditions, free of direct anthropogenic influence, can be found. It has been referred to as the "Green Ocean," since particle concentrations can be as low as that is seen over the ocean and, like the marine atmosphere, small changes in particle properties can have a major impact on clouds and climate (Andreae et al., 2004). While isoprene is the most abundantly emitted biogenic volatile organic compound (BVOC), monoterpenes and sesquiterpenes are observed in significant amounts as to potentially influence particle composition (Alves et al., 2016). While, on an annual basis, aerosol particle sources in the Amazon basin are dominated by the oxidation of BVOCs by OH and O_3, in many parts of the Amazon, anthropogenic emissions of trace gases and oxidants, as well as human-caused-biomass burning, can have a significant impact (Martin et al., 2010; de Sá et al., 2017, 2019). Biomass burning events, both for land clearing as well as pasture and cropland maintenance, can produce particles at high number and mass concentrations. Increased urbanization in the Amazon, for example the city of Manaus, Brazil, with a 2017 population of 2.1 million, represents large area sources of emissions of both gases and particles and has led to increased regional transportation infrastructure and resulting increases in oxides of nitrogen (NOx) (IBGE, 2017). The latter will have important implications on the reactive pathways of BVOCs and the formation of secondary organic aerosol (SOA) (de Sá et al., 2018). With the ability to observe aerosol particles under pristine conditions, combined with the presence of growing urban centers and increased land use change that represent significant regional sources of oxidants and other key trace gases, this region presents opportunities to understand both past and future drivers of atmospheric chemistry and climate.

Aerosol properties in the Amazon basin show a seasonal dependence, reflecting seasonal variability in emissions and

deposition. During the wet season (December through March), the region is dominated by natural emissions, as accumulation and coarse mode particles tend to be lower in concentration due to wet deposition (Andreae, 2009). In the wet season, ambient particle number concentrations often represent pristine, background concentrations and are in the range of 300-600 cm^3 (Zhou et al., 2002). Previous measurements of particle number-size distributions in Amazonia during the wet season show ultrafine particles are present intermittently, most likely linked to times of local pollution events, while both Aitken and accumulation mode are continuously present (Zhou et al., 2002). While the wet season episodically experiences high particle number concentrations, the dry season (June through September) experiences larger number concentrations most of the time, which can alter cloud microphysics, radiative effects and influences the hydrological cycle (Andreae et al., 2002, 2004; Rcia et al., 2000). While it was previously thought that particle composition during the dry period is dominated by biomass burning, recent measurements of sub-micron particle (PM_1) composition show a larger influence from BVOCs due to decreased wet deposition, resulting in positive feedbacks on oxidants and emissions (de Sá et al., 2019). Seasonal variations of isoprene, sesquiterpenes and monoterpenes have been measured, with higher mixing ratios in the dry season (Alves et al., 2016). Additionally, with the lack of rainfall, in-basin pollution may be more prevalent, especially in areas downwind of cities and settlements (Martin et al., 2010).

Unlike other forested regions, particles with a diameter smaller than 30 nm are rarely observed over the Amazon basin, suggesting that new particle formation events seldom occur near the ground (Martin et al., 2010). In other regions, new particle formation has been seen to occur during the daytime under sunny conditions, suggesting that both boundary layer dynamics and photochemistry are important factors (Bzdek et al., 2011). Rizzo et al. (2018) recently analyzed four years of particle size distributions acquired at the TT34 tower site located 60 km northwest of Manaus. Regional new particle formation and growth events were detected in only 3% of days, whereas bursts of ultrafine particles that lasted as least an hour occurred during 28% of the days. Those “burst events” were equally likely to occur during the daytime as the night, and the authors hypothesized that daytime events were caused by interrupted photochemical new particle formation, whereas nocturnal events might be due to emissions of primary biological particles. Recent airborne observations in the Amazon suggest that particle nucleation and growth can be initiated in the upper troposphere, with upwelling air masses transporting reactants into the free troposphere and downwelling air masses transporting aerosol particles and condensable compounds back into the boundary layer where particles can continue to grow via condensation and coagulation (Andreae et al., 2018; Fan et al., 2018; Wang et al., 2016). Once formed, ultrafine particles can have an oversized impact on atmospheric processes. One recent study by Fan et al. (2018) has suggested that ultrafine particles can increase the convective intensity of deep convective clouds. High concentrations of ultrafine particles, when present with high water vapor concentrations that are typical in the Amazon atmosphere, can form high concentrations of small cloud droplets that release latent heat and thereby result in more powerful updraft velocities.

While recent research is providing some clarity on the origin, transport, and climate impacts of ultrafine particles in the Amazon, very little is known about the chemical composition of these particles. Globally, measurements show a major component of atmospheric ultrafine aerosol are organic compounds produced from BVOC oxidation (Bzdek et

al., 2011; Riipinen et al., 2012; Smith et al., 2008; Smith and Rathbone, 2008). Many of these direct measurements of the composition of atmospheric ultrafine particles have been performed using the Thermal Desorption Chemical Ionization Mass Spectrometer (TDCIMS) (Voisin et al., 2003). For example, TDCIMS measurements performed outside of Mexico City attribute about 90% of the growth of freshly nucleated particles to oxidized organics (Smith et al., 2008). In the Boreal forest of Finland, the contribution of oxidized organics is close to 100% and an analysis of composition suggests that marine emissions can play an important role in that process (Lawler et al., 2018). For the smallest particles measureable by TDCIMS, with diameters from 8 to 10 nm, between 23% to 47% of the constituents may be derived from organic salt formation, a reactive uptake mechanism that requires the presence of strong bases such as gas phase amines (Smith et al., 2010).

Similar to other parts of the world, particles in the Amazon basin are typically composed of 70-80% organics by mass in both the fine and coarse size ranges (Graham et al., 2003). The composition of ultrafine particles has not been directly measured, although one study has proposed the major component could be oxidized organics that have condensed onto potassium salt-rich primary particles emitted from active biota (Pöhlker et al., 2012). An understanding of the origin and chemical composition of ultrafine particles in the Amazon gives insight into their formation and growth processes. To improve upon modelling the coupling of chemistry and climate in this sensitive region, incorporating accurate representations of particle formation and growth process is required.

The most recent, and currently the largest, field campaign to study the Amazon atmospheric chemistry and cloud processes was the Observations and Modeling of the Green Ocean Amazon (GoAmazon2014/5), which took place outside of Manaus, from 1 January 2014 to 31 December 2015 (Martin et al., 2016). Two intensive observational periods (IOPs) were carried out during GoAmazon2014/5, corresponding to wet and dry seasons in 2014. This manuscript explores the chemical composition of ultrafine particles observed by the TDCIMS during IOP1, which took place from February 1 to March 31, 2014. Specifically, we focus on ten consecutive days that experienced air mass from both clean, remote regions as well as from the large metropolitan region of Manaus. This study investigates the influence of anthropogenic and biogenic emissions on the chemical composition of ultrafine particles in this region, from which one can infer the chemical processes that led to the formation and growth of ambient ultrafine particles in this region. The time evolution of select compounds in ambient ultrafine particles is analyzed, and compared to AMS measurements, using Principal Component Analysis (PCA), in order to gain additional insights into the contribution of various emission sources to ultrafine particle composition.

2. Methodology

2.1 T3 Site Description

All data presented were collected at the T3 site (3.2133 ºS, 60.5987 ºW), located 70 km west of Manaus, Brazil, during the GoAmazon2014/5 campaign (Martin et al., 2016). The T3 site is located within pasture land located 10 km northeast of Manacapuru, Brazil. The site included the Atmospheric Radiation Measurement (ARM) Mobile Facility #1 (AMF-1), the ARM Mobile Aerosol Observing System (MAOS), and four modified shipping container laboratories containing instruments deployed by universities and other research organizations.

144 **2.2 Thermal Desorption Chemical Ionization Mass Spectrometry**

145 Characterization of ambient ultrafine particle composition was obtained using TDCIMS. The TDCIMS is an
146 instrument designed specifically for the measurement of the molecular composition of size-resolved ultrafine aerosol
147 particles (Smith et al., 2004; Voisin et al., 2003). In brief, sampled atmospheric particles are charged by a unipolar
148 charger and are collected via electrostatic deposition on a platinum (Pt) filament over varying collection times. During
149 this campaign, collection times were either for 1 hour or 30 minutes, depending on the anticipated sample mass.
150 Typical sample mass collected on the filament ranged from 10 to 100 ng. After collection, the filament was moved
151 into an atmospheric pressure chemical ionization source region and resistively heated to desorb the particulate phase
152 components. These desorbed components were chemically ionized and detected using a quadrupole mass spectrometer
153 (Extrel Corp.). A zero air generator (Parker Hannifin, model HPZA-3500) provided the source of reagent ions
154 $(H_2O)_nH^+$ and $(H_2O)_nO_2^-$ (n=1-3); TDCIMS operation with these ion chemistries are, respectively, referred to as
155 positive and negative ion modes. Complete mass spectra of desorbed compounds were obtained at the beginning of
156 IOP1 (Fig. S1) to determine ions with the highest ion abundances. These ions were then measured for the duration of
157 the campaign by operating the quadrupole mass spectrometer in "selected ion mode," in which the quadrupole mass
158 spectrometer rapidly switched among approximately 12 ions to optimize sensitivity with high temporal resolution.

159 Both positive and negative ion mode chemical analyses were performed during the two IOPs, and are publicly
160 available on the campaign data archive (Smith, 2016). During IOP1, several days of measurements were impacted by
161 intermittent power outages and brownouts. IOP2 was characterized by low concentrations of ultrafine particles, which
162 is consistent with prior observations (Martin et al., 2010; Rizzo et al., 2018). Because of this, we focus our analysis
163 on ten consecutive days during IOP1 when instruments were operating consistently. This period also happened to
164 coincide with the arrival of two distinct and consecutive air masses, which allows for more accurate side-by-side
165 comparison of aerosol properties during these periods.

166 Ambient particles were sampled through a 3 m length of Cu tubing with 0.63 cm inside diameter. The inlet extended
167 0.5 m above the roof of the laboratory, and was bent and covered with screen to prevent rain and insects from entering.
168 Ambient particles during GoAmazon2014/5 were not size-selected prior to collection on the filament because of low
169 ambient concentrations. The collection process, however, is inherently dependent on particle mobility (McMurry et
170 al., 2009). In order to determine the size-dependent collection efficiency, tests were run at the start of the campaign
171 by generating and collecting ammonium sulfate particles in the diameter range of 8-90 nm. The size-dependent
172 collection efficiency was used to determine the volume mean diameter and estimated mass of each sample.

173 **2.3 Meteorological data and complementary datasets**

174 To complement the TDCIMS dataset, High-Resolution Time-of-Flight Aerosol Mass Spectrometry (AMS; Aerodyne,
175 Inc.) was used to characterize non-refractory compounds in PM_1 at the T3 site (ARM, 2018d.; de Sá et al., 2018). A
176 Scanning Mobility Particle Sizer (ARM, 2018b) determined the number-size distributions spanning the mobility
177 diameter range of 10 - 460 nm. Eight-hour back-trajectory simulations were determined for the time period of interest
178 using NOAA HYSPLIT transport model, using the GDAS 1° meteorology (Rolph et al., 2017; Stein et al., 2015).
179 Wind direction, wind speed, relative humidity, temperature and rainfall were measured at AMF-1 (ARM, 2018c) and

the planetary boundary layer height (ARM, 2018a), determined using the Heffter number method (Heffter, 1980), was measured at MAOS.

2.4 Principal Component and Hierarchical clustering analyses

Principal Component Analysis (PCA) was performed using the "princomp" function of the R statistical software package (R, 2011). A hierarchical cluster analysis is performed using Ward's averaging method in the "hclust" function in R. Ward's minimum variance method of hierarchical clustering was used, which groups species within the same cluster to minimize the total variance (Wilks, 2011). The purpose of this analysis is to identify species or groups of species that may have unique sources, trajectories or other physicochemical characteristics. Cluster analysis was done for the following TDCIMS negative and positive ion mode species: $C_2H_4N^-$ (*m/z* 42), $C_2H_3O_2^-$ (*m/z* 59), HSO_4^- (*m/z* 97), Cl^- (isotopes *m/z* 35 and 37), $HC_2O_4^-$ (*m/z* 89), $NH_4^+(H_2O)$ (*m/z* 36), K^+ (*m/z* 39 and 41), $C_3H_{10}N^+$ (*m/z* 60), $C_5H_7O^+$ (*m/z* 83), $C_5H_8NO^+$ (*m/z* 98), and $C_7H_9O_2^+$ (*m/z* 125) and the following AMS species: organic, ammonium, nitrate, sulfate and chloride. A separate cluster analysis was performed for quality assurance and demonstrated that the three clusters presented in Section 3.3 are statistically significant and different from one another.

3. Results and Discussion

3.1 Meteorological Data and Classification of Air Masses

The ten consecutive days that are the focus of this study can be characterized by two distinct air mass types, as determined from meteorological data and AMS-derived PMF factors (de Sá et al., 2018). The first period, referred to as the "anthropogenic period," was from 14 March until mid-morning 19 March and the second period, the "background period," was from mid-morning 19 March until 24 March. The AMS-derived biomass burning factor (BBOA), associated with levoglucosan, and anthropogenic-dominated factor (ADOA), associated with mass fragment 91 or "91fac" ($C_7H_7^+$), were as much as three times larger during the anthropogenic period than background period (de Sá et al., 2018). Anthropogenic influence during this campaign, as determined using ADOA, most strongly resembled cooking emissions. Correlations between the ADOA factor, cooking emissions, aromatics like benzene, toluene and xylene and increased particle counts verify the link to anthropogenic influence from Manaus (de Sá et al., 2018). The particle number-size distribution, shown in Figure 1, for the anthropogenic period saw higher number concentrations of particles over the diameter range of 10 – 200 nm. The average total mass concentration as determined by the AMS for the anthropogenic period was 2.5 ± 0.9 μg/m^3. The T3 site experienced approximately four hours of rain on 19 March ending at about noon UTC (all times are presented as UTC time, which is four hours ahead of local time) and the first and only new particle formation event of this ten-day period was observed. After this event on 19 March, number concentrations of particles were, on average, much lower than the prior period. The average total mass concentration for the background period was determined to be 1.2 ± 0.8 μg/m^3. A similar trend in total mass concentration between background and polluted conditions was observed during the Southern Oxidant and Aerosol Study (SOAS), where larger particle mass concentrations were observed during times with polluted air mass influence and, when followed by a period of rainfall, smaller mass concentrations were observed (Liu and Russell, 2017).

Atmos. Chem. Phys. Discuss., https://doi.org/10.5194/acp-2019-299
Manuscript under review for journal Atmos. Chem. Phys.
Discussion started: 24 April 2019

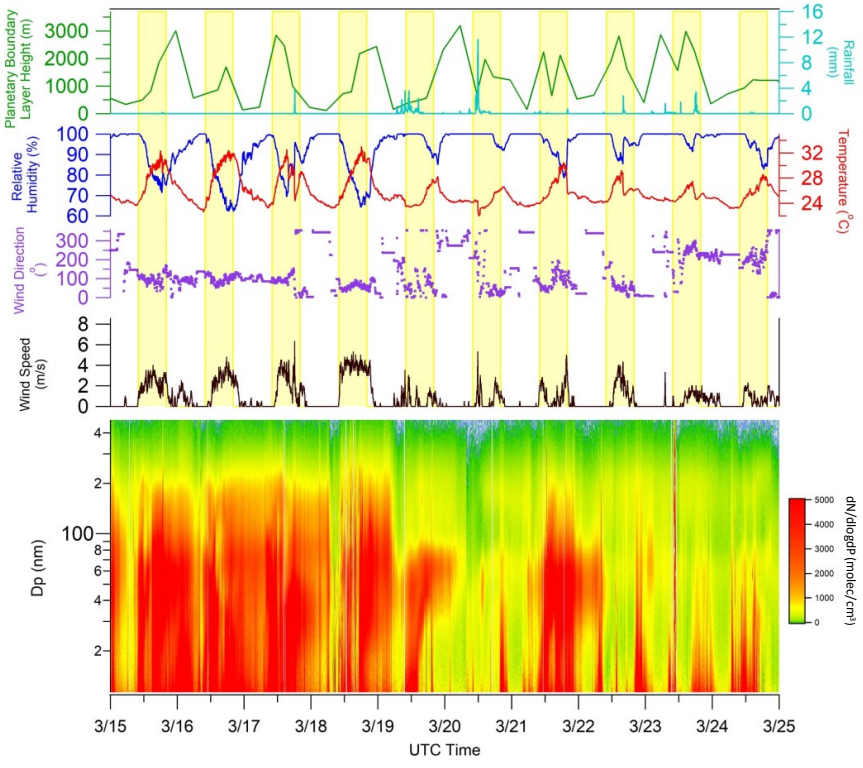

Figure 1: Meteorological data from the T3 site, showing planetary boundary layer height (green), rainfall (light blue), relative humidity (dark blue), temperature (red), wind direction (purple) and wind speed (black). The highlighted yellow bars signify daylight hours (10:00-22:00, UTC time). The particle number- size distribution contour plot shows size distribution function (molecules cm^{-3}) for particles sizes between 10 nm and 400 nm.

Occasional rainfall was seen during the background period, resulting in wet deposition of aerosol particles. Addtionally, a backtrajectory analysis, presented next, provides a more likely reason for these two distinct periods.

Wind direction data shown in Figure 1, as well as NOAA HYSPLIT data shown in Figure 2, suggest a reason for the two distinct periods. Back-trajectories show that air masses during the anthropogenic period either pass through Manaus or south of Manaus prior to arrival at the T3 site. During this period, air masses often also pass over the main roadway that connects Manaus with Manacapuru, a neighbouring city with a population of 93,000. Along this roadside are homes, agriculture and brick kilns, all of which contribute to local gas and particle emissions. In contrast, during the background period, air masses arrived at the T3 site from the northeast to northwest ~70% of the time (Figure 2). During the evening of 21 March there was a period of increased number concentration and, as winds were quite stagnant at night, it is possible that a local emission source could have impacted the site during that period.

Estimated masses of ultrafine particles sampled by the TDCIMS were determined and compared for the two periods (Fig. S2). During the anthropogenic period there was no distinct diurnal pattern observed, with an average of ~100

Atmos. Chem. Phys. Discuss., https://doi.org/10.5194/acp-2019-299
Manuscript under review for journal Atmos. Chem. Phys.
Discussion started: 24 April 2019

Atmospheric Chemistry and Physics Discussions

ng/sample. This lack of a diurnal pattern in the sampled particles suggests that sources or processes that are responsible for these particles could have persisted throughout the day and night or could be from different processes that persisted both day and night. In contrast to this, the background period has a diurnal peak in estimated mass collected between 18:00 to 22:00 UTC, with sampled masses of ~70 ng/sample. The minimum sample sizes occurred in the early morning where averages reached as low as 16 ng/sample. Peaks in collected mass during the early afternoon could be linked to photochemically produced sources and appear to be unique to the background period.

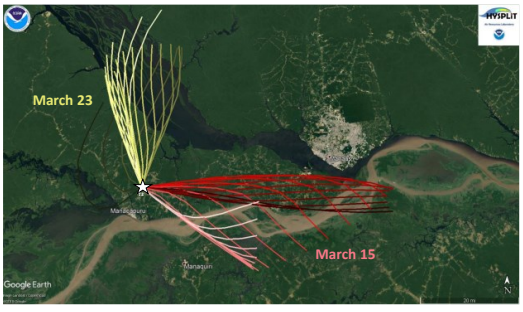

Figure 2: Back trajectories were performed using HYSPLIT to show the difference between the types of air masses that travel to the T3 site during the anthropogenic period (red traces) and biogenic period (yellow traces). Each set of traces show 8-hour back trajectories every 1 hour during the day denoted. The lightest color indicates the first back trajectory on the denoted day arriving to the T3 site at midnight and the darkest color indicates the last back trajectory arriving to the T3 site at 23:00. Image data: Google Earth

3.2 Ultrafine particle chemical composition

The five most abundant negative ions, as observed in full mass spectra (Fig. S1) taken at the start of the wet season campaign, are attributed to $C_2H_4N^-$ (organic nitrogen species, *m/z* 42), $C_2H_3O_2^-$ (acetate, *m/z* 59), HSO_4^- (bisulfate, *m/z* 97), Cl^- (chloride, isotopes *m/z* 35 and 37) and $HC_2O_4^-$ (hydrogen oxalate, *m/z* 89). The six most abundant positive ions measured were attributed to $NH_4^+(H_2O)$ (ammonium hydrate, *m/z* 36), K^+ (potassium, isotopes *m/z* 39 and 41), $C_3H_{10}N^+$ (trimethyl ammonium, *m/z* 60), $C_5H_7O^+$ (protonated 3-methylfuran, *m/z* 83), $C_5H_8NO^+$ (*m/z* 98), and $C_7H_9O_2^+$ (*m/z* 125). We will refer to $C_5H_8NO^+$ (*m/z* 98), and $C_7H_9O_2^+$ (*m/z* 125) collectively as "other" in our positive ion mode analysis as these were minor components. The major isotopes of chloride were measured to understand the role chloride may have had on particle formation, with potential influence from marine aerosol and fungal spores (Pöhlker et al., 2012). Potassium (isotopes *m/z* 39 and 41) was measured during positive ion mode analysis to determine the potential influence of potassium-rich primary biological particles (China et al., 2016; Pöhlker et al., 2012). Mass-normalized ion abundances, defined as ion abundance divided by collected sample mass, for the five most abundant negative ions displayed similar diurnal patterns within each period. During the anthropogenic period, peaks in mass-normalized ion abundance were observed for all measured species between 6:00-8:00 and 16:00-18:00. For the background period, there was no sharp peak observed between 16:00-18:00 for any of the five measured species, but peak in the diurnal pattern between 6:00-8:00 for *m/z* 42, *m/z* 59 and *m/z* 89 (Fig. S3). Diurnal trends in mass-normalized ion abundances give little insight, per se, into sources of individual ions, but it is interesting to note that ion abundances are typically the lowest when sample mass is largest. A potential reason for this is that TDCIMS is not sensitive to the specific compounds present in these ultrafine particles when the mass loading is highest. This could be true, for example, if refractory black carbon is the main constituent during the period of highest sampled mass, as chemical ionization would be unable to detect these compounds. Since the diurnal patterns of all individual ions are similar, a comparison of ion fractions, defined as ion abundance divided by the sum of the total ion abundances measured at the time of analysis, provides a measurement of ion concentration in collected particles and shows distinct differences between the background and anthropogenic periods.

Atmos. Chem. Phys. Discuss., https://doi.org/10.5194/acp-2019-299
Manuscript under review for journal Atmos. Chem. Phys.
Discussion started: 24 April 2019

Atmospheric Chemistry and Physics Discussions

263 Figure 3a shows the trend in ion fraction for five most abundant negative ions and four most abundant positive ions
264 during the ten-day period of analysis. During the anthropogenic period, the observed bisulfate ion (*m/z* 97) fraction
265 was larger than during the background period. Of the ions measured, bisulfate is the predominant indicator of urban
266 influence. The bisulfate anion has been previously noted in TDCIMS analysis as a stable ion formed from the thermal
267 desorption of particulate sulfate (Voisin et al., 2003), and it is likely that emissions from Manaus could serve as the
268 major source for sulfate found at the T3 site. Thus as air masses during the anthropogenic period primarily traveled

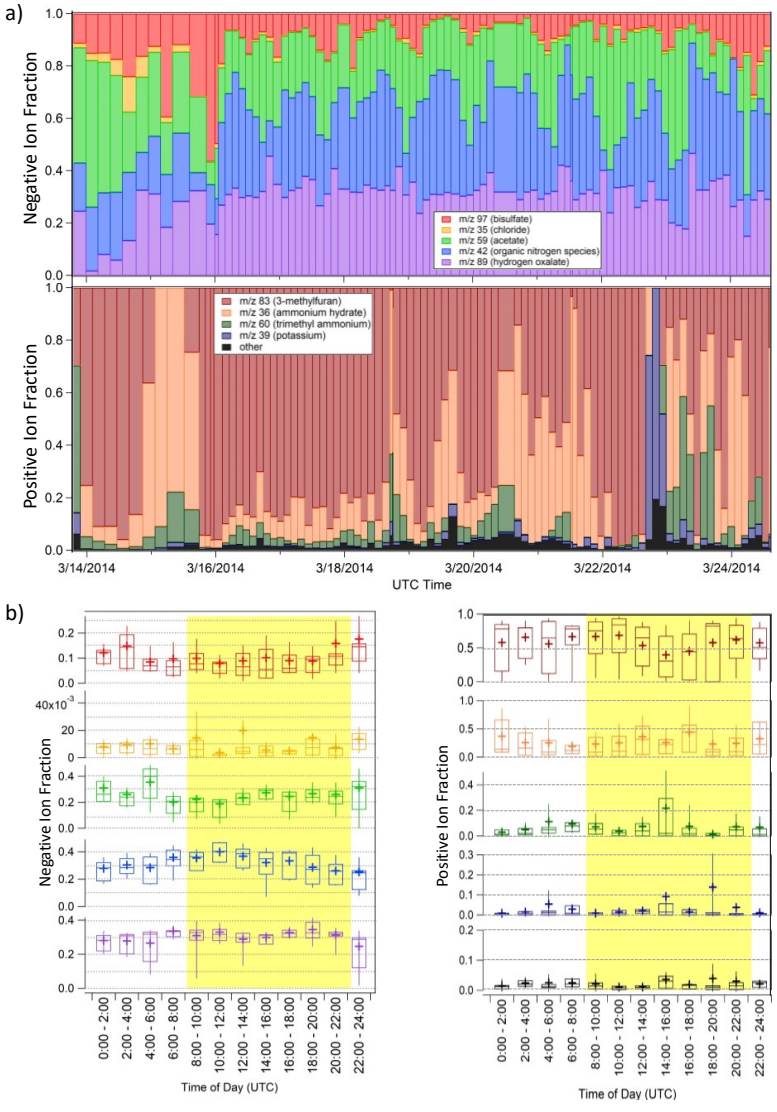

Figure 3: a) The negative ion fraction and positive ion fraction shown over the ten-day period of interest. b) Diel patterns of the five measured negative ions shown and of the four major positive ions, "other" refers to sum of fractions of m/z 125 and m/z 98. Highlighted region denotes daylight hours.

from, or south of, Manaus, bisulfate is expected to have a higher measured ion fraction. When the bisulfate ion was the largest of the negative ions, the largest fractions of ammonium (*m/z* 36) and trimethyl ammonium (*m/z* 60) in the positive ion mode were observed as well. Additionally, the largest chloride (*m/z* 35) signal was observed at the beginning of this period, reaching a maximum of about 10% of the total ion fraction on 14 March. During the background period, the ion fraction of hydrogen oxalate (*m/z* 89) remained relatively constant, averaging 31% ± 5% of the total ion fraction. Diurnal patterns of these ion fractions, shown in Figure 3b, show small diurnal variations for most of the observed ions. The diurnal pattern of *m/z* 42 (organic nitrogen species) peaks between 10:00 and noon and both *m/z* 59 and *m/z* 89 show slight decreases between 10:00 and noon, as well. Roughly 70% of measurements over both periods had potassium (*m/z* 39 and 41) ion fractions less than or equal to 20% of the total positive ion fraction, with few "potassium episodes" of higher abundance observed.

Interestingly, *m/z* 42 was the most abundant ion present in TDCIMS spectra. Due to its even mass-to-charge ratio, this ion almost certainly contains nitrogen. This ion distinguishes itself from other detected compounds by a peak in ion fraction during the morning (Figure 3b). Prior TDCIMS measurements during the 2006 MILAGRO campaign in the Mexico City Metropolitan Area, detected *m/z* 42 as a major ion fragment in sub-20 nm diameter particles; that ion was identified at that time as cyanate (CNO^-), which may be linked to biomass burning or industrial processes (Smith et al., 2008). However, the *m/z* 42 fragment observed in this study is not likely cyanate since this ion was observed during very clean periods when we expect anthropogenic emissions and biomass burning to be low. In addition, TDCIMS-measured *m/z* 42 during the dry season did not show an increase in ion intensity relative to the wet season (Smith, 2016), which one might expect if this ion were sourced to biomass burning. We hypothesize that this ion is the organic nitrogen species $C_2H_4N^-$, which is associated with background emissions of amino or other water soluble organic species as reported by Mace, et al. (2003). That study, performed on particulate matter smaller than 10 μm in aerodynamic diameter (PM_{10}) collected in 1999, found that organic nitrogen compounds were a major constituent in particles during the wet season in the Amazon basin. Amino acids and other proteinaceous material have been measured in the gas phase, particle phase and in precipitation across the globe, which has been estimated to account for as much as 55-95% of particulate matter over the Amazon basin (Artaxo et al., 1988, 1990; Zhang and Anastasio, 2003). In addition, a recent analysis of the composition of sub-2.5 μm particulate matter ($PM_{2.5}$) collected during GoAmazon2014/5 and analyzed by high resolution mass spectrometry found that organic nitrogen species were second most abundant compound class, with oxidized organics first (Kourtchev et al., 2016). If true, these observations suggest that organic nitrogen compounds play a crucial role in both ultrafine particle formation as well as growth to large particles, which make this mechanism for particle growth climatologically important in this region.

Of the measured positive ion species, *m/z* 83, linked to 3-methylfuran or other C5 oxidized volatile organic compound, dominated the ion fraction in ultrafine particles. Methylfuran has been observed to be produced as a thermal decomposition product of isoprene-derived SOA via AMS measurements (Allan et al., 2014), a process that would likely also occur during TDCIMS analysis. Airborne observations in the Amazon suggest that isoprene SOA can be formed in the boundary layer under certain conditions, which is confirmed by these observations (Allan et al., 2014). Since this ion is a marker of isoprene epoxydiol (IEPOX) species present in the particle phase, this confirms a role for

isoprene and isoprene derivatives in the growth of ultrafine particles. The diel pattern of methylfuran peaks at 8:00-10:00, linking this ion to potential photochemical sources. It is important to note that this ion dominates the positive ions fraction during both the anthropogenic and background influenced periods. Times that experienced lower fractions of *m/z* 83 had increased fractions of ammonium and trimethyl ammonium, which also coincided at times with larger amounts of measured bisulfate in the negative ions. The presence of larger fractions of particulate ammonia and amines at times with less influence from isoprene-derived species could indicate that both organic salt formation and uptake of isoprene-derived products are possible mechanisms of ultrafine particle growth. The importance of organic salt formation in growth is consistent with prior TDCIMS measurements (Smith et al., 2010), although a quantitative comparison cannot be made since this current study focuses on sub-100 nm diameter particles whereas the prior study focused on size-resolved sub-15 nm ambient particles. One period of elevated potassium ion ratio, believed to be connected to potassium-rich biological particles or the rupturing of biological spores (China et al., 2016; Pöhlker et al., 2012), was observed at the end of the day on 22 March. Of all wet season TDCIMS measurements during GoAmazon2014/5, roughly 14% of measurements had potassium fractions greater than 0.1 (Fig. S4). Air masses on the evening of 22 March were traveling steadily from the Manaus area and coincided with about 5 mm of rain. High ambient concentrations of biological particles that could be sources of potassium are often associated with rainfall events (China et al., 2016). Rupturing of fungal spores, leading to the production of sub-100 nm fragments, was observed to occur after long exposures (above 10 hours) of high relative humidity and subsequent drying, similar conditions to those on 22 March.

3.3 Multivariate analysis of TDCIMS and AMS data

Principal Component Analysis (PCA) was performed on TDCIMS and AMS measurements to provide insights into the possible drivers for ultrafine particle formation. Figure 4 shows the results of this analysis. In these plots, positive correlations are shown in blue, while negative correlations are shown in red. The intensity of the color and eccentricity of the ellipse is an indication of the degree of correlation. Pale-colored circles (eccentricity approximately 0) show little to no correlation, narrow ellipses with a positive slope and darker blue color illustrate strong positive correlations and narrow ellipses with a negative slope and darker red color show strong negative correlation.

Hierarchical clustering of these measurements results in three main clusters of related particle constituents. This represents a series of clusters where the species within each cluster covary, therefore indicative, in this work, of similar particle characteristics, processes or sources. The first, labeled “Cluster 1” on Figure 4, grouped TDCIMS-derived organic nitrogen species (*m/z* 42), acetate (*m/z* 59) hydrogen oxalate (*m/z* 89), trimethyl ammonium (*m/z* 60) and 3-methylfuran (*m/z* 83); the second, labeled “Cluster 2,” clustered well known co-varying AMS derived constituents (Ulbrich et al., 2009); the third, labeled “Cluster 3” associated AMS-derived chloride with TDCIMS-derived chloride (*m/z* 35), bisulfate (*m/z* 97), ammonium hydrate (*m/z* 36) and potassium (*m/z* 39). The hierarchical clustering approach independently grouped and separated AMS measurements from TDCIMS measurements. While both represent composition measurements of the aerosol population, the differences between the size ranges of particles measured

Atmos. Chem. Phys. Discuss., https://doi.org/10.5194/acp-2019-299
Manuscript under review for journal Atmos. Chem. Phys.
Discussion started: 24 April 2019

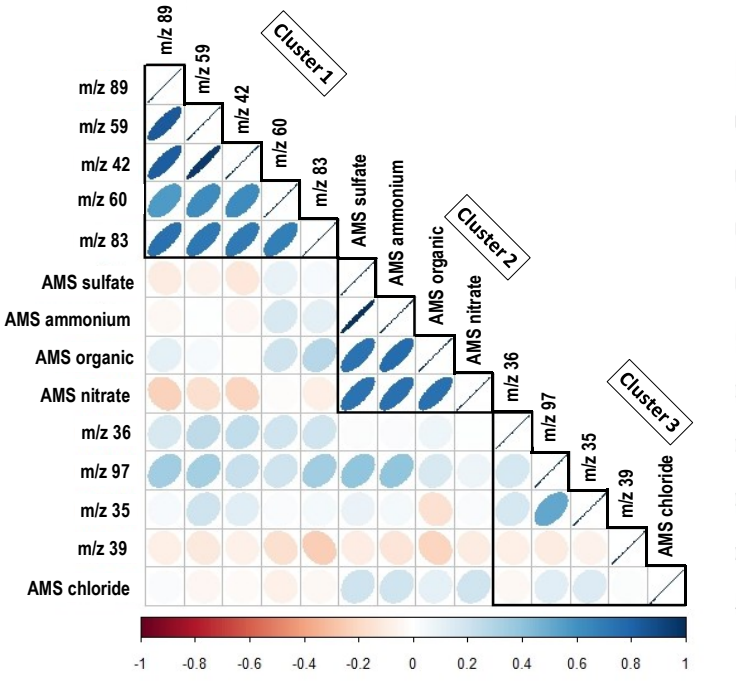

Figure 4: Principal Component Analysis (PCA) of TDCIMS and AMS data. Refer to text for details on the interpretation of these plots. PCA results in which species are grouped into hierarchical clusters, with clusters denoted within weighted black lines. Species are ordered by decreasing correlation to the first principal component from the top to bottom.

by AMS and TDCIMS techniques would lead to the anticipated differences in clustering. Comparing mass distributions estimated by size distribution measurements, the presence of particles larger than 100 nm would have a more significant contribution to the measured mass concentrations by AMS. In contrast, the TDCIMS only measures sub-100 nm particles, representing a minor contribution to the total mass concentration. This observed separation between the clustering of AMS and TDCIMS measurements reinforces the importance of direct measurements of ultrafine particles, as opposed to bulk composition, in accessing the species and mechanisms responsible for new particle formation.

With respect to PCA performed on the two datasets, Cluster 1, which includes TDCIMS fragments typically linked to organic species (*m/z* 59, 89, 83) and nitrogen species discussed previously (*m/z* 42 and 60), explains most of the variance and has the highest correlation with the first principal component. These species' high correlation with each other indicate similar sources, most of which can be associated with BVOC emissions. A prior TDCIMS laboratory study linked the acetate ion fragment (*m/z* 59) to particulate carboxylic and dicarboxylic acids (Smith and Rathbone, 2008), which have been linked to the photochemical oxidation of both biogenic and anthropogenic compounds (Winkler et al., 2012). During the wet season in the Amazon basin, specific dicarboxylic acids and tricarboxylic acids

and have been identified and proposed to have been formed from the oxidation of semi-volatile fatty acids and terpenes (Kubátová et al., 2000). Hydrogen oxalate, measured as *m/z* 89, was one of the two most abundant organic ions measured in ultrafine particles at both an urban and rural site in Helsinki, Finland (Pakkanen et al., 2000). Hydrogen oxalate was noted to have relatively constant concentrations in ultrafine particles, similar to observations seen during the ten-day period of analysis for this study (Figure 3). While Helsinki and the Amazon experience different conditions and meteorology, oxalate has been observed in both environments, possibly due to the heavy BVOC influence in both locales. In the positive ion mode, 3-methylfuran, measured as *m/z* 83, has significant correlation to background linked negative ions. These species seem to be generally linked to the oxidation of various BVOCs, whether isoprene, for 3-methylfuran, or other terpenes (Allan et al., 2014). Finally, it should be noted that the clustering of the organic nitrogen species (*m/z* 42) with these organic ions provides further evidence that the source of this ion is likely clean, background chemistry rather than from biomass burning.

Hierarchical clustering separates TDCIMS-measured ions into two clusters, with Cluster 3 including TDCIMS-derived bisulfate (*m/z* 97), chloride (*m/z* 35 and 37), ammonium hydrate (*m/z* 36) and potassium (*m/z* 39 and 41). The separation of this cluster suggests that these constituents are linked to different sources or atmospheric processes compared to those in Cluster 1, potentially with an anthropogenic origin as both chloride and bisulfate have been linked previously to biomass burning and anthropogenic emissions, respectively (Allen and Miguel, 1995; Martin et al., 2010; Voisin et al., 2003). As noted previously, the bisulfate anion is stable ion formed from the thermal desorption of particulate sulfate (Voisin et al., 2003) and it is likely present in ultrafine particles via pollution emissions from Manaus. Additionally, in-basin emissions of various gaseous precursors like dimethyl sulfide and hydrogen sulfide could contribute to particulate sulfate of non-anthropogenic origin, as bisulfate was measured during the whole ten-day period of interest, even without observed direct influence from Manaus. In-basin chloride emissions could come from both biomass burning of common regional vegetation and long range transport of marine ultrafine particles from the Atlantic Ocean under influence of the Trade Winds (Allen and Miguel, 1995; Martin et al., 2010). The production of potassium, which is potentially linked to the rupturing of fungal spores, would have little correlation to other measured TDCIMS species, as the presence of potassium is dependent on ambient conditions, like rain and relative humidity. This ion is not generally associated to constant background sources, like TDCIMS species observed in Cluster 1, or associated with potential anthropogenic sources, like bisulfate and chloride seen in Cluster 3. The clustering of TDCIMS ion abundances into two clusters suggests different sources and processes for these species, as there is little correlation between the species present in Cluster 1 to those present in Cluster 3.

4. Conclusion

The chemical composition of ultrafine particles in the Amazon basin, as measured during the GoAmazon2014/5, has two distinct influences: sources and processes linked to anthropogenic origin and those related to background sources and processes. During periods of heavier anthropogenic influence, higher number concentrations of sub-100 nm particles were observed (Figure 1). HYSPLIT back trajectories during the anthropogenic period (Figure 2) not only intersect with the Manaus metropolitan area, but with the main roadway that connects Manaus with the city of

Manacapuru. Influence from anthropogenic sources, which during the study period are primarily linked to Manaus metropolitan area emissions, may continuously affect the composition of ultrafine particles observed at the T3 measurement site. Particulate sulfate, measured as the bisulfate ion, was an important and dominant contributor to TDCIMS ion fraction during the anthropogenic period (Figure 3), but was still measured, to a lesser extent, in the background period, suggesting an omnipresent influence. The most abundant species measured during this campaign, which we hypothesize to be organic nitrogen species at *m/z* 42, displayed a consistent morning diurnal peak and was an equally abundant constituent during both the anthropogenic and background periods. The dominance of this ion during both this study and the 2006 MILAGO campaign in the Mexico City Metropolitan Area emphasizes the potential role of organic nitrogen in ultrafine aerosol particle formation and underscore the need for further research into the chemical processes and precursors that are responsible for this ion. 3-Methylfuran, measured as *m/z* 83, was the most dominant fraction observed in the positive ion mode and is likely associated with IEPOX derivatives present in ultrafine particles. The presence of these species emphasizes the important of isoprene oxidation to particle formation in this region. The two different clusters of TDCIMS-derived ions that arise through PCA analysis, of which Cluster 1 explains most of the variance, give additional insight into the sources and processes that influence the ultrafine particle population in this part of the Amazon basin. As hierarchical clustering separates TDCIMS-derived organic species from TDCIMS-derived sulfate and chloride, this suggests these species are present in the particle from different sources and/or processes. A third cluster separates AMS-measured compounds from those detected by TDCIMS, which emphasizes the unique characteristics of ultrafine particles compared to bulk aerosol particles. The lack of correlation between the two TDCIMS-derived clusters supports the observation that anthropogenic emissions and processes have a unique role to play in ultrafine particle formation and growth in the Amazon basin.

Author contributions

JNS, PA, STM, OVB, RdS, and JT designed the measurement campaign and JNS, MJL, JO, SSdS carried out measurements. HSG performed data analysis, assisted by JNS and AC. HSG prepared the manuscript with contributions from all co-authors.

Competing interests

The authors declare that they have no conflict of interest.

Acknowledgements

Institutional support was provided by the Central Office of the Large Scale Biosphere Atmosphere Experiment in Amazonia (LBA), the National Institute of Amazonian Research (INPA), and Amazonas State University (UEA) and the local Research Support Foundation (FAPEAM/GOAMAZON). We acknowledge support from the Atmospheric Radiation Measurement (ARM) Climate Research Facility, a user facility of the United States Department of Energy, Office of Science, sponsored by the Office of Biological and Environmental Research, and support from the

420 Atmospheric System Research (ASR, DE-SC0011122 and DE-SC0011115) program of that office. JS acknowledges
421 support from a Brazilian Science Mobility Program (Programa Ciência sem Fronteiras) Special Visiting Researcher
422 Scholarship. PA acknowledges funding from FAPESP – Fundação de Apoio à Pesquisa do Estado de São Paulo,
423 Grants number 2017/17047-0, 2013/05014-0 and 2014/50848-9.

424 **References**

425 Allan, J. D., Morgan, W. T., Darbyshire, E., Flynn, M. J., Williams, P. I., Oram, D. E., Artaxo, P., Brito, J., Lee, J. D.
426 and Coe, H.: Airborne observations of IEPOX-derived isoprene SOA in the Amazon during SAMBBA, Atmos. Chem.
427 Phys, 14, 11393–11407, doi:10.5194/acp-14-11393-2014, 2014.

428 Allen, A. G. and Miguel, A. H.: Biomass Burning in the Amazon: Characterization of the ionic component of aerosols
429 generated from flaming and smouldering rainforest and savannah, Environ. Sci. Technol., 29, 486–493, 1995.

430 Alves, E. G., Jardine, K., Tota, J., Jardine, A., Maria Yãnez-Serrano, A., Karl, T., Tavares, J., Nelson, B., Gu, D.,
431 Stavrakou, T., Martin, S., Artaxo, P., Manzi, A. and Guenther, A.: Seasonality of isoprenoid emissions from a primary
432 rainforest in central Amazonia, Atmos. Chem. Phys, 16, 3903–3925, doi:10.5194/acp-16-3903-2016, 2016.

433 Andreae, M. O.: Correlation between cloud condensation nuclei concentration and aerosol optical thickness in remote
434 and polluted regions, Atmos. Chem. Phys., 9(2), 543–556, doi:10.5194/acp-9-543-2009, 2009.

435 Andreae, M. O., Artaxo, P., Brandão, C., Carswell, F. E., Ciccioli, P., Costa, A. L. da, Culf, A. D., Esteves, J. L.,
436 Gash, J. H. C., Grace, J., Kabat, P., Lelieveld, J., Malhi, Y., Manzi, A. O., Meixner, F. X., Nobre, A. D., Nobre, C.,
437 Ruivo, M. d. L. P., Silva-Dias, M. A., Stefani, P., Valentini, R., Jouanne, J. von and Waterloo, M. J.: Biogeochemical
438 cycling of carbon, water, energy, trace gases, and aerosols in Amazonia: The LBA-EUSTACH experiments, J.
439 Geophys. Res., 107(D20), 8066, doi:10.1029/2001JD000524, 2002.

440 Andreae, M. O., Rosenfeld, D., Artaxo, P., Costa, A. A., Frank, G. P., Longo, K. M. and Silva-Dias, M. A. F.: Smoking
441 Rain Clouds over the Amazon, Science (80-.)., 303(5662), 1337–1342, 2004.

442 Andreae, M. O., Afchine, A., Albrecht, R., Amorim Holanda, B., Artaxo, P., Barbosa, H. M. J., Borrmann, S.,
443 Cecchini, M. A., Costa, A., Dollner, M., Fütterer, D., Järvinen, E., Jurkat, T., Klimach, T., Konemann, T., Knote, C.,
444 Krämer, M., Krisna, T., Machado, L. A. T., Mertes, S., Minikin, A., Pöhlker, C., Pöhlker, M. L., Pöschl, U., Rosenfeld,
445 D., Sauer, D., Schlager, H., Schnaiter, M., Schneider, J., Schulz, C., Spanu, A., Sperling, V. B., Voigt, C., Walser, A.,
446 Wang, J., Weinzierl, B., Wendisch, M. and Ziereis, H.: Aerosol characteristics and particle production in the upper
447 troposphere over the Amazon Basin, Atmos. Chem. Phys, 18, 921–961, doi:10.5194/acp-18-921-2018, 2018.

448 ARM: Atmospheric Radiation Measurement (ARM) Climate Research Facility. 2013, updated hourly. Planetary
449 Boundary Layer Height (PBLHTSONDE1MCFARL). 2014-03-10 to 2014-03-10, ARM Mobile Facility (MAO)
450 Manacapuru, Amazonas, Brazil; AMF1 (M1). Compiled by C. Sivar, 2018a.

451 ARM: Atmospheric Radiation Measurement ARM Climate Research Facility. 2014, updated hourly. Scanning
452 mobility particle sizer (AOSSMPS). 2014-03-13 to 2014-03-24, ARM Mobile Facility (MAO) Manacapuru,
453 Amazonas, 2018b.

454 ARM: Wind speed, wind direction, temperature, precipitation and relative humidity during GoAmazon2014/5, data
455 portal: https://iop.archive.arm.gov/arm-iop/2014/mao/goamazon/T3/springston-met/, last access: 27 June 2018,
456 2018c.

457 ARM: Aerosol Mass Spectrometer Particle Composition measurements during GoAmazon2014/5, data portal:
458 https://iop.archive.arm.gov/arm-iop/2014/mao/goamazon/T3/alexander-ams/, last access: 27 June 2018, n.d.

459 Artaxo, P., Storms, H., Bruynseels, F., Grieken, R. V. and Maenhaut, W.: Composition and Sources of Aerosols From
460 the Amazon Basin, J. Geophys. Res., 93(D2), 1605–1615, 1988.

461 Artaxo, P., Maenhaut, W., Storms, H. and Van Grieken, R.: Aerosol characteristics and sources for the Amazon Basin
462 during the wet season, J. Geophys. Res., 95(D10), 16971, doi:10.1029/JD095iD10p16971, 1990.

Bzdek, B. R., Zordan, C. A., Luther III, G. W., Johnston, M. V and Luther, G. W.: Nanoparticle Chemical Composition During New Particle Formation, Aerosol Sci. Technol., 458(45), doi:10.1080/02786826.2011.580392, 2011.

Carlton, A. G., T Pye, H. O., Baker, K. R. and Hennigan, C. J.: Additional Benefits of Federal Air-Quality Rules: Model Estimates of Controllable Biogenic Secondary Organic Aerosol, , doi:10.1021/acs.est.8b01869, 2018.

China, S., Wang, B., Weis, J., Rizzo, L., Brito, J., Cirino, G. G., Kovarik, L., Artaxo, P., Gilles, M. K. and Laskin, A.: Rupturing of Biological Spores As a Source of Secondary Particles in Amazonia, Environ. Sci. Technol, 50, 12179–12186, doi:10.1021/acs.est.6b02896, 2016.

Fan, J., Rosenfeld, D., Zhang, Y., Giangrande, S. E., Li, Z., Machado, L. A. T., Martin, S. T., Yang, Y., Wang, J., Artaxo, P., Barbosa, H. M. J., Braga, R. C., Comstock, J. M., Feng, Z., Gao, W., Gomes, H. B., Mei, F., Pöhlker, C., Pöhlker, M. L., Pöschl, U. and De Souza, R. A. F.: Substantial convection and precipitation enhancements by ultrafine aerosol particles, Science (80-.)., 359(6374), 411–418, doi:10.1126/science.aan8461, 2018.

Graham, B., Guyon, P., Maenhaut, W., Taylor, P. E., Ebert, M., Matthias-Maser, S., Mayol-Bracero, O. L., Godoi, R. H. M., Artaxo, P., Meixner, F. X., Moura, M. A. L., Rocha, C. H. E. D., Grieken, R. Van, Glovsky, M. M., Flagan, R. C. and Andreae, M. O.: Composition and diurnal variability of the natural Amazonian aerosol, J. Geophys. Res. Atmos., 108(D24), n/a-n/a, doi:10.1029/2003JD004049, 2003.

Heffter, J. L.: Transport Layer Depth Calculations, in Second Joint Conference on Applications of Air Pollution Meteorology, p. New Orleans, Louisiana., 1980.

Hofmann, D. J.: Climate Forcing by Anthropogenic Aerosols, Science (80-.)., 255(5043), 423–430, doi:10.1126/science.255.5043.423, 2015.

IBGE, B. I. of G. and S.: IBGE releases population estimates for municipalities in 2017., 2017.

Intergovernmental Panel on Climate Change: Climate Change 2013: The Physical Science Basis. Contribution of Working Group 1 to the Fifths Assessment Report of the Intergovernmental Panel on Climate Change., 2013.

Jimenez, J. L., Canagaratna, M. R., Donahue, N. M., Prevot, A. S. H., Zhang, Q., Kroll, J. H., DeCarlo, P. F., Allan, J. D., Coe, H., Ng, N. L., Aiken, A. C., Docherty, K. S., Ulbrich, I. M., Grieshop, A. P., Robinson, A. L., Duplissy, J., Smith, J. D., Wilson, K. R., Lanz, V. A., Hueglin, C., Sun, Y. L., Tian, J., Laaksonen, A., Raatikainen, T., Rautiainen, J., Vaattovaara, P., Ehn, M., Kulmala, M., Tomlinson, J. M., Collins, D. R., Cubison, M. J., Dunlea, J., Huffman, J. A., Onasch, T. B., Alfarra, M. R., Williams, P. I., Bower, K., Kondo, Y., Schneider, J., Drewnick, F., Borrmann, S., Weimer, S., Demerjian, K., Salcedo, D., Cottrell, L., Griffin, R., Takami, A., Miyoshi, T., Hatakeyama, S., S., A., Sun, J. Y., Zhang, Y. M., Dzepina, K., Kimmel, J. R., Sueper, D., Jayne, J. T., Herndon, S. C., Trimborn, A. M., Williams, L. R., Wood, C., E., Middlebrook, A. M., Kolb, C. E., Baltensperger, U. and Worsnop, D. R.: Evolution of organic aerosols in the atmosphere, Science (80-.)., 326, 1525–1529, 2009.

Kourtchev, I., Godoi, R. H. M., Connors, S., Levine, J. G., Archibald, A. T., Godoi, A. F. L., Paralovo, S. L., Barbosa, C. G. G., Souza, R. A. F., Manzi, A. O., Seco, R., Sjostedt, S., Park, J. H., Guenther, A., Kim, S., Smith, J., Martin, S. T. and Kalberer, M.: Molecular composition of organic aerosols in central Amazonia: An ultra-high-resolution mass spectrometry study, Atmos. Chem. Phys., 16(18), 11899–11913, doi:10.5194/acp-16-11899-2016, 2016.

Kubátová, A., Vermeylen, R., Claeys, M., Cafmeyer, J., Maenhaut, W., Roberts, G. and Artaxo, P.: Carbonaceous aerosol characterization in the Amazon basin, Brazil: Novel dicarboxylic acids and related compounds, in Atmospheric Environment, vol. 34, pp. 5037–5051., 2000.

Lawler, M. J., Rissanen, M. P., Ehn, M., Mauldin, R. L., Sarnela, N., Sipilä, M. and Smith, J. N.: Evidence for Diverse Biogeochemical Drivers of Boreal Forest New Particle Formation, Geophys. Res. Lett., 45(4), 2038–2046, doi:10.1002/2017GL076394, 2018.

Liu, J. and Russell, L. M.: Observational evidence for pollution-influenced selectiveuptake contributing to biogenic secondary organicaerosols in the southeastern U.S., Geophys. Res. Lett., 44, 8056–8064, 2017.

Mace, K. A., Artaxo, P. and Duce, R. A.: Water-soluble organic nitrogen in Amazon Basin aerosols during the dry (biomass burning) and wet seasons, J. Geophys. Res., 108(D16), 4512, doi:10.1029/2003JD003557, 2003.

508 Martin, S. T., Andreae, M. O., Artaxo, P., Baumgardner, D., Chen, Q., Goldstein, A. H., Guenther, A., Heald, C. L.,
509 Mayol-Bracero, O. L., McMurry, P. H., Pauliquevis, T., Pschl, U., Prather, K. A., Roberts, G. C., Saleska, S. R., Silva
510 Dias, M. A., Spracklen, D. V., Swietlicki, E. and Trebs, I.: Sources and properties of Amazonian aerosol particles,
511 Rev. Geophys., 48(2), doi:10.1029/2008RG000280, 2010.

512 Martin, S. T., P.Artaxo, Machado, L. A. T., Manzi, A. O., Souza, R. A. F., C.Schumacher, Wang, J., Andreae, M. O.,
513 Barbosa, H. M. J., Fan, J., G.Fisch, Goldstein, A. H., Guenther, A., Jimenez, J. L., Pöschl, U., Dias, M. A. S., J.N.
514 Smith, A. and Wendisch, M.: Introduction: Observations and Modeling of the Green Ocean Amazon
515 (GoAmazon2014/5), Atmos. Chem. Phys., 16, 4785–4797, 2016.

516 McMurry, P. H., Ghimire, A., Ahn, H.-K., Sakurai, H., Moore, K., Stolzenburg, M. and Smith, J. N.: Sampling
517 Nanoparticles for Chemical Analysis by Low Resolution Electrical Mobility Classification, Environ. Sci. Technol.,
518 43, 4653–4658, doi:10.1021/es8029335, 2009.

519 Pakkanen, T. A., Korhonen, C. H., Hillamo, R. E., Aurela, M., Aarnio, P., Koskentalo, T. and Maenhaut, W.: Ultrafine
520 particles (PM0.1) in the Helsinki area, J. Aerosol Sci., 31(Supplement 1), 522–523, doi:10.1016/S0021-
521 8502(00)90535-4, 2000.

522 Pöhlker, C., Wiedemann, T., Sinha, B., Shiraiwa, M., Gunthe, S., Smith, M., Su, H., Artaxo, P., Chen, Q., Cheng, Y.,
523 Elbert, W., Gilles, M., Kilcoyn, A., Moffet, R., Weigand, M., Martin, S., Pöschl, U. and Andreae, M.: Biogenic
524 Potassium Salt Particles as Seeds for Secondary Organic Aerosol in the Amazon, Science (80-.)., 337(6098), 1075–
525 1078, 2012.

526 R, D. C. T.: R: A Language and Environment for Statistical Computing, R Found. Stat. Comput., 1(2.11.1), 409,
527 doi:10.1007/978-3-540-74686-7, 2011.

528 Rcia, M., Yamasoe, A., Artaxo, P., Miguel, A. H. and Allen, A. G.: Chemical composition of aerosol particles from
529 direct emissions of vegetation in the Amazon Basin: water-soluble species and trace elements, Atmos. Environ., 34,
530 1641–1653, 2000.

531 Riipinen, I., Yli-Juuti, T., Pierce, J. R., Petäjä, T., Worsnop, D. R., Kulmala, M. and Donahue, N. M.: The contribution
532 of organics to atmospheric nanoparticle growth, Nat. Publ. Gr., 5, doi:10.1038/NGEO1499, 2012.

533 Rizzo, L. V., Roldin, P., Brito, J., Backman, J., Swietlicki, E., Krejci, R., Tunved, P., Petäjä, T., Kulmala, M. and
534 Artaxo, P.: Multi-year statistical and modeling analysis of submicrometer aerosol number size distributions at a rain
535 forest site in Amazonia, Atmos. Chem. Phys, 18, 10255–10274, doi:10.5194/acp-18-10255-2018, 2018.

536 Rolph, G., Stein, A. and Stunder, B.: Real-time Environmental Applications and Display sYstem: READY, Environ.
537 Model. Softw., 95, 210–228, doi:10.1016/j.envsoft.2017.06.025, 2017.

538 de Sá, S. S., Palm, B. B., Campuzano-Jost, P., Day, D. A., Newburn, M. K., Hu, W., Isaacman-VanWertz, G., Yee,
539 L. D., Thalman, R., Brito, J., Carbone, S., Artaxo, P., Goldstein, A. H., Manzi, A. O., Rodrigo A. F. Sou, A. and
540 Martin, S. T.: Influence of urban pollution on the production of organic particulate matter from isoprene epoxydiols
541 in central Amazonia, Atmos. Chem. Phys., 17, 6611–6629, 2017.

542 de Sá, S. S., Palm, B. B., Campuzano-Jost, P., Day, D. A., Hu, W., Isaacman-VanWertz, G., Yee, L. D., Brito, J.,
543 Carbone, S., Ribeiro, I. O., Cirino, G. G., Liu, Y. J., Thalman, R., Sedlacek, A., Funk, A., Schumacher, C., Shilling,
544 J. E., Schneider, J., Artaxo, P., Goldstein, A. H., Souza, R. A. F., Wang, J., McKinney, K. A., Barbosa, H., Alexander,
545 M. L., Jimenez, J. L., Martin, S. T. and Suzane S. de Sá, Brett B. Palm, Pedro Campuzano-Jost, Douglas A. Day,
546 Weiwei Hu, Gabriel Isaacman-VanWertz, Lindsay D. Yee, Joel Brito, Samara Carbone, Igor O. Ribeiro, Glauber G.
547 Cirino, Yingjun J. Liu, Ryan Thalman, Arthur Sedlacek, Aaron Funk, Courtney, S. T. M.: Urban influence on the
548 concentration and composition of submicron particulate matter in central Amazonia, Atmos. Chem. Phys., 1–56,
549 doi:10.5194/acp-2018-172, 2018.

550 de Sá, S. S., Campuzano-Jost, P., Palm, B. B., Barbosa, H. M. J., Yee, L. D., Brito, J., Liu, Y. J., Artaxo, P., Jimenez,
551 J. L., Goldstein, A. H., Day, D. A., Alexander, M. L., Springston, S., Martin, S. T., Carbone, S., Rizzo, L. V, Wernis,
552 R., Sedlacek, A. and Isaacman-VanWertz, G.: Contributions of biomass-burning, urban, and biogenic emissions to
553 the concentrations and light-absorbing properties of particulate matter in central Amazonia during the dry season,
554 Atmos. Chem. Phys. Discuss., 1–77, doi:10.5194/acp-2018-1309, 2019.

555 Shrivastava, M., Cappa, C. D., Fan, J., Goldstein, A. H., Guenther, A. B., Jimenez, J. L., Kuang, C., Laskin, A., Martin,
556 S. T., Ng, N. L., Petaja, T., Pierce, J. R., Rasch, P. J., Roldin, P., Seinfeld, J. H., Shilling, J., Smith, J. N., Thornton,
557 J. A., Volkamer, R., Wang, J., Worsnop, D. R., Zaveri, R. A., Zelenyuk, A. and Zhang, Q.: Recent advances in
558 understanding secondary organic aerosol: Implications for global climate forcing, Rev. Geophys., 55(2), 509–559,
559 doi:10.1002/2016RG000540, 2017.

560 Smith, J. N.: Thermal Desorption Chemical Ionization Mass Spectrometry during GoAmazon2014/5, data portal,
561 2016.

562 Smith, J. N. and Rathbone, G. J.: Carboxylic acid characterization in nanoparticles by thermal desorption chemical
563 ionization mass spectrometry, Int. J. Mass Spectrom., 274, 8–13, 2008.

564 Smith, J. N., Moore, K. F., McMurry, P. H. and Eisele, F. L.: Atmospheric Measurements of Sub-20 nm Diameter
565 Particle Chemical Composition by Thermal Desorption Chemical Ionization Mass Spectrometry, Aerosol Sci.
566 Technol., 38(2), 100–110, doi:10.1080/02786820490249036, 2004.

567 Smith, J. N., Dunn, M. J., VanReken, T. M., Iida, K., Stolzenburg, M. R., McMurry, P. H. and Huey, L. G.: Chemical
568 composition of atmospheric nanoparticles formed from nucleation in Tecamac, Mexico: Evidence for an important
569 role for organic species in nanoparticle growth, Geophys. Res. Lett., 35(4), 2–6, doi:10.1029/2007GL032523, 2008.

570 Smith, J. N., Barsanti, K. C., Friedli, H. R., Ehn, M., Kulmala, M., Collins, D. R., Scheckman, J. H., Williams, B. J.
571 and McMurry, P. H.: Observations of aminium salts in atmospheric nanoparticles and possible climatic implications,
572 Proc. Natl. Acad. Sci., 107(15), 6634–6639, doi:10.1073/pnas.0912127107, 2010.

573 Stein, A. F., Draxler, R. R., Rolph, G. D., Stunder, B. J. B., Cohen, M. D. and Ngan, F.: Noaa's hysplit atmospheric
574 transport and dispersion modeling system, Bull. Am. Meteorol. Soc., 96(12), 2059–2077, doi:10.1175/BAMS-D-14-
575 00110.1, 2015.

576 Ulbrich, I. M., Canagaratna, M. R., Q. Zhang, D. R. W. and Jimenez, J. L.: Interpretation of organic components from
577 Positive Matrix Factorization of aerosol mass spectrometric data, Atmos. Chem. Phys., 9, 2891–2918, 2009.

578 Voisin, D., Smith, J. N., Sakurai, H., Mcmurry, P. H., Eisele, F. L. and D. Voisin, J.N. Smith, H. Sakurai, P.H.
579 McMurry, F. L. E.: Thermal Desorption Chemical Ionization Mass Spectrometer for Ultrafine Particle Chemical
580 Composition, Aerosol Sci. Technol., 37(37), 471–475, doi:10.1080/02786820390125232, 2003.

581 Wang, J., Krejci, R., Giangrande, S., Kuang, C., Barbosa, H. M. J., Brito, J., Carbone, S., Chi, X., Comstock, J., Ditas,
582 F., Lavric, J., Manninen, H. E., Mei, F., Moran-Zuloaga, D., Pöhlker, C., Pöhlker, M. L., Saturno, J., Schmid, B.,
583 Souza, R. A. F., Springston, S. R., Tomlinson, J. M., Toto, T., Walter, D., Wimmer, D., Smith, J. N., Kulmala, M.,
584 Machado, L. A. T., Artaxo, P., Andreae, M. O., Petäjä, T. and Martin, S. T.: Amazon boundary layer aerosol
585 concentration sustained by vertical transport during rainfall, Nat. Publ. Gr., 539, doi:10.1038/nature19819, 2016.

586 Wilks, D. S.: Statistical methods in the atmospheric sciences, Elsevier/Academic Press., 2011.

587 Winkler, P. M., Ortega, J., Karl, T., Cappellin, L., Friedli, H. R., Barsanti, K., McMurry, P. H. and Smith, J. N.:
588 Identification of the biogenic compounds responsible for size-dependent nanoparticle growth, Geophys. Res. Lett.,
589 39(20), 1–6, doi:10.1029/2012GL053253, 2012.

590 Zhang, Q. and Anastasio, C.: Free and combined amino compounds in atmospheric fine particles (PM 2.5) and fog
591 waters from Northern California, Atmos. Environ., 37, 2247–2258, doi:10.1016/S1352-2310(03)00127-4, 2003.

592 Zhou, J., Swietlicki, E., Hansson, H. C. and Artaxo, P.: Submicrometer aerosol particle size distribution and
593 hygroscopic growth measured in the Amazon rain forest during the wet season, J. Geophys. Res. D Atmos., 107(20),
594 doi:10.1029/2000JD000203, 2002.

595

596